INFRARED PHOTOMETRY OF THE GLOBULAR CLUSTER PALOMAR 6

Jae-Woo Lee[1,2,3] & Bruce W. Carney[1,4]

ABSTRACT

We present JHK photometry of Palomar 6. Our photometric measurements range from the RGB-tip to $\approx$ 2 mag below the RHB and our CMDs show that Palomar 6 appears to have a well-defined RHB population. The distance modulus and interstellar reddening of the cluster are estimated by comparing the magnitude and color of Palomar 6 RHB stars with respect to those of 47 Tuc. We obtain $(m-M)_0 = 14.28$ mag and $E(B-V) = 1.30$ mag for the cluster and our study suggests that Palomar 6 is clearly located in the Galaxy's central regions. We also discuss the metallicity of the cluster using the slope of the RGB. We obtain [Fe/H] ≈ -1.2 for Palomar 6 and our metallicity estimate is $\approx$ 0.5 - 1.0 dex lower than previous estimates by others.

Subject headings: globular clusters: individual (Palomar 6) — infrared: stars

1. Introduction

Palomar 6 ($\alpha = 17^h\ 44^m$, $\delta = -26°\ 13'$; $l = 2.1°$, $b = 1.8°$; J2000) is a globular cluster $\approx$ 0.8 kpc from the Galactic center and $\approx$ 0.2 kpc from the plane (Harris 1996). Since it lies near the Galactic center, it is highly reddened.

---

[1]Department of Physics & Astronomy, University of North Carolina, Chapel Hill, NC 27599-3255; jaewoo@astro.unc.edu; bruce@physics.unc.edu

[2]Center for Space Astrophysics, Yonsei University, Shinchon-dong 134, Seoul 120-749, Korea

[3]PMA Division, California Institute of Technology, Mail Stop 405-47, Pasadena, CA 91125, USA; jaewoo@srl.caltech.edu

[4]Visiting Astronomer, Kitt-Peak National Observatory, National Optical Astronomy Observatory, which is operated by the Association of Universities for Research in Astronomy, Inc., under contract with the National Science Foundation.

Malkan (1981) derived the interstellar reddening for Palomar 6, $E(B-V) = 1.4$, based on a reddening-free metallicity index Q_{IR}.[5] Ortolani, Bica, & Barbuy (1995) obtained $E(B-V)$ = 1.33 ± 0.10 based on the VI color magnitude diagram (CMD). Bica et al. (1998) also studied the cluster employing intermediate resolution (5.4 Å pixel^{-1}) integrated spectra and they derived the smallest value of the interstellar reddening value for the cluster, $E(B-V)$ = 1.25.

The metallicity of the cluster is rather controversial. Malkan (1981) obtained a metallicity of [Fe/H] = −1.30 for Palomar 6 using the Q_{IR} index, ranking it an intermediate metallicity inner halo cluster. Zinn (1985) derived [Fe/H] = −0.74 for Palomar 6 by re-analyzing Malkan's photometry. Ortolani et al. (1995) estimated [Fe/H] ≈ −0.4 based on the VI CMD. Minniti (1995) studied the metallicities of seven reddened clusters including Palomar 6. He obtained spectra of six red-giant branch (RGB) stars in Palomar 6 with a 2 Å resolution covering $\lambda\lambda$ 4700 – 5400 Å. He suggested that the sum of Mg λ 5175 Å, Fe λ 5270 Å, and Fe λ 5535 Å lines (Mg + 2Fe) is the most sensitive to metallicity following Faber et al. (1985), and he derived [Fe/H] = +0.2 ± 0.3 for Palomar 6 based on the location of the giants in the Mg + 2Fe *vs* $(J-K)_0$ diagram. More recently, Bica et al. (1998) obtained $[Z/Z_\odot] = -0.09$ by measuring Ca II triplet $\lambda\lambda$ 8498, 8542, and 8662 Å using the intermediate resolution integrated spectra.

As discussed above, Palomar 6 suffers a large interstellar reddening. The interstellar extinction in the visual passband A_V for Palomar 6 is expected to be ≈ 3.9 – 4.3 mag, depending on its true interstellar reddening value, and the apparent visual magnitude of the horizontal branch (HB) V_{HB} is ≈ 20 mag (Ortolani et al. 1995). Thus, photometric study of Palomar 6 in the visual passband is very difficult. It is also likely that differential reddening, which is commonly detected in heavily reddened clusters, is present. The IR photometry is, therefore, essential for studying Palomar 6, since it is less sensitive to the interstellar reddening and the differential reddening effect. In this paper, we explore the ground-based JHK photometry of Palomar 6. A comparison with JK photometry of Minniti, Olszewski, Rieke (1995) is made. The distance modulus using the K magnitude of the red horizontal branch (RHB) and the metallicity estimate using the RGB slope of the cluster are discussed.

[5] Q_{IR} is defined to be H_2O + 1.5 CO, where H_2O and CO are the narrow-band infrared photometric absorption indices from H_2O at 2.0 μm and CO at 2.4 μm. Malkan (1981) claimed that there is a correlation between Q_{IR} and a reddening-free ultraviolet line-blanketing parameter Q_{39} (Zinn 1980) with, $Q_{IR} = 0.045 + 0.45 Q_{39}$.

2. Observations and IR data reduction techniques

Our observations were carried out using the 4m telescope at KPNO on the night of June 15 1997 under photometric conditions. The detector was a 256×256 HgCdTe NICMOS3 array and the JHK filter system was employed. The image scale was 0.60 arcsec pixel^{-1} providing a field of view (FOV) of 2.56 × 2.56 arcmin. The journal of observations is presented in Table 1.

During our observations, we dithered the telescope pointing to minimize the effects induced by bad pixels and cosmic ray events. For standard star frames, the telescope pointing was dithered with an offset of 37 arcsec between successive exposures. Offsets of 6 and 10 arcsec were applied for Palomar 6 object frames.

NICMOS3 detectors utilize a hybrid architecture in which each pixel has an associated unit cell which controls the biasing and readout of the pixel. Thus, each pixel is essentially independent of the others and charge bleeding or trailing from saturated pixels is not present. However, this independence also means that such properties as linearity and dark current can vary from pixel to pixel, and it is necessary to calibrate these effects for optimum scientific performance.

The mean dark current of NICMOS3 is known to be $\approx 2\ e^{-1}$/sec. However it does not scale simply with the exposure time. Thus we obtained dark frames with the same exposure times as object and standard star frames to calibrate the dark currents.

The non-linearity of the detector sensitivity was also calibrated. We obtained a series of dome flats with exposure times of 3, 10, 15, 20, and 30 sec maintaining the same illumination intensity. We also obtained 1 sec exposures before and after each exposure to monitor possible changes in the illumination. Then the fluxes of each exposure were normalized to that of 1 sec exposures. The measured fluxes for each exposure were plotted as a function of expected fluxes with linear sensitivity. Then we derived a third-order relation,

$$ADU_{corr} = ADU_{obs}[0.9952 + 0.0744\frac{ADU_{obs}}{32767} - 0.0489(\frac{ADU_{obs}}{32767})^2], \quad (1)$$

where ADU_{corr} and ADU_{obs} are the corrected flux and the observed flux in ADU, respectively. This relation was then applied to each object frame using the IRAF[6] task IRLINCOR. Figure 1 shows the non-linear response curve of NICMOS3 detector. The solid line represents

[6] IRAF (Image Reduction and Analysis Facility) is distributed by the National Optical Astronomy Observatory, which is operated by the Association of Universities for Research in Astronomy, Inc., under contract with the National Science Foundation.

the linear relation and filled circles represent the observed fluxes and open circles represent the corrected fluxes using the relation above.

The sky-flats were generated by median-combining object frames of the individual dithering sequences for each passband. This procedure essentially removes the stellar light and cosmic ray, and provides good sky-flats for less crowded fields, such as standard star frames. The sky-flats generated using Palomar 6 object frames, however, show residuals of stellar images, indicating that this procedure fails when the field is too crowded. Applying sky-flats generated from the other images taken at different times may cause potential problems. It is known that there are two predominant sources of infrared sky background, which are essentially independent, both physically and spectrally. At short wavelengths (in particular H passband), the sky is dominated by emission lines from OH in the upper atmosphere (typically 90 km altitude). The strength of these lines can vary over the course of a night; in addition, upper level winds create inhomogeneity and motion of the airglow. As a result, the intensity of the background can vary unpredictably during the night. At longer wavelengths, thermal emission from the telescope optics and optically thick telluric lines predominates. The transition between these two regimes occurs at approximately 2.3 microns, so the background with filters other than K' or K is primarily OH airglow. We produced master sky-flats, which were median-combined sky-flats of the whole set of standard star frames, rather than using sky-flats from a single dithering sequence. Since the standard star frames were taken over the night in our observation, using these master sky-flats will minimize the risk of the abrupt changes of infrared sky background.

Figure 2 shows a comparison between the sky-flat generated using the Palomar 6 frame (upper left) and our master sky-flat (upper right) in the J passband. As can be seen, the sky-flat using the Palomar 6 frames shows residuals of stellar light. This causes serious problems in the central part of the cluster, where the field is more crowded. The flat-field corrected images are also shown in the Figure. The lower left panel shows the final image using the sky-flat from the Palomar 6 frames and the lower right panel shows that of using the master sky-flat. The former does not resolve fainter stars very well and even brighter stars were turned out to be affected by the residual flux on the sky flat in the central part of the cluster. Therefore, we used the master sky-flat in our analysis.

It is known that there are several hundred bad pixels in the NICMOS3 detector used in our observation. The bad pixel correction was applied after the flat-field correction step. The bad pixel mask was generated using the standard star frames. The flat-field corrected standard star frames ($\approx$ 100 frames) were normalized and then median combined. Since the strict definition of a bad pixel is rather subjective except for the non-responsive (dead) pixels, the pixels deviating more than 7 σ around the mean value (= 1.0) were defined to be bad pixels. The pixel values at the bad pixel position were interpolated using those of nearby pixels. Finally, the object frames in each dithering sequence were combined. Our combined image of Palomar 6 in K passband is shown in Figure 3.

During the night, we observed the six UKIRT faint standard stars (Casali & Hawarden 1992). It should be noted that the number of IR standard stars is small and the most of the IR standard stars by Elias et al. (1982) are too bright for our camera plus telescope configuration. All standard frames were analyzed using the PHOTOMETRY task in DAOPHOTII (Stetson 1995). With the results of aperture photometry, growth curve analysis was performed using DAOGROW (Stetson 1990) to obtain integrated magnitudes.

The extinction coefficients were derived from one standard star (FS25). The first-order K passband extinction term k_k is 0.101 mag airmass^{-1} and the first-order color extinction terms k'_{jk} and k'_{jh} are -0.004 and 0.045 mag airmass^{-1}, respectively.

To calibrate the photometry, the photometric transformations were assumed to have the following form,

$$\begin{aligned} K_{UKIRT} &= k_0 + \zeta_K, \\ (J-K)_{UKIRT} &= \mu(j-k)_0 + \zeta_{J-K}, \\ (J-H)_{UKIRT} &= \epsilon(j-h)_0 + \zeta_{J-H}. \end{aligned} \tag{2}$$

The transformation coefficients are $\zeta_K = -3.235 \pm 0.010$, $\mu = 0.957 \pm 0.019$, $\zeta_{J-K} = 0.624 \pm 0.007$, $\epsilon = 1.006 \pm 0.016$, and $\zeta_{J-H} = 0.156 \pm 0.004$ in the UKIRT JHK system. (The errors are those of the mean.) Figure 4 shows the residuals of K_{UKIRT}, $(J-K)_{UKIRT}$, and $(H-K)_{UKIRT}$ using these transformation coefficients. The mean values are 0.000 ± 0.010 in the K_{UKIRT} passband, 0.000 ± 0.010 in the $(J-K)_{UKIRT}$ color, and 0.000 ± 0.007 in the $(H-K)_{UKIRT}$ color. (The errors are those of the mean.)

Point-spread function (PSF) photometry for all Palomar 6 frames was performed using DAOPHOTII and ALLSTAR/ALLFRAME (Stetson 1987, 1994, 1995; Turner 1995). The first step was to perform the aperture photometry with star lists returned from the FIND routine. We calculated PSFs using isolated bright stars. To obtain good PSFs on each frame, at least 3 iterations of neighboring-star removal were performed. For the PSF calculations, we adopted a spatially invariable PSF since, unlike modern CCDs, a NICMOS3 array has a small FOV, so that the stellar radial profiles are not expected to show large variations over the frame. Also, the number of PSF stars is too small (usually 20-30 stars) to calculate reliable variable PSFs in each frame. In case of 2K CCD system, the number of PSF stars are large enough (for example 90-110 stars in Lee & Carney 1999) to calculate a variable PSF in each frame. After the first ALLFRAME pass, we undertook an additional pass to find more stars on the subtracted frames. Since we used a small PSF radius (usually, $\approx 4\times$FWHM) to compute the PSF magnitude due to crowding, a PSF magnitude must be converted into an aperture magnitude with a larger radius, a process known as *aperture correction*. The 20 to 30 PSF stars on each frame were used for this purpose. Comparisons of the PSF magnitude and the aperture magnitude from the growth-curve method yielded aperture corrections. Finally airmass corrections and photometric transformations were applied.

To convert the UKIRT JHK system to the CIT JHK system, we used the following transformation equations given by Casali & Hawarden (1992),

$$\begin{aligned} K &= K_{UKIRT} - 0.018(J-K)_{UKIRT}, \\ (J-K) &= 0.936(J-K)_{UKIRT}, \\ (H-K) &= 0.960(H-K)_{UKIRT}. \end{aligned} \tag{3}$$

3. Results and discussions

3.1. Color Magnitude Diagrams

Our composite CMDs of Palomar 6 are presented in Figure 5 and the sample CMD data are shown in Table 2. In the Table, the positions (columns 2 and 3) are presented in pixel units (0.60 arcsec pixel^{-1}). The CMD data are available upon request to the authors or the electronic version of the journal. Off-cluster field populations were not obtained during our observation, therefore, the field star contamination is not removed in our CMDs. Since Palomar 6 lies near the Galactic center, the off-cluster field contamination is expected to be very high (see below), and probably variable due to differential reddening.

Our photometric measurements range from the RGB-tip to $\approx$ 2 mag below the RHB. The most prominent feature in our CMDs is a well-defined RHB morphology at $H \approx 13.5$ mag and $K \approx 13.3$ mag. The scatter in the RGB sequences appear to be larger in $(J-K)$ than in $(J-H)$. This is most likely due to the bright sky background in the K passband.

3.2. Comparison with the IR photometry of Minniti, Olszewski, & Rieke

Minniti, Olszewski, & Rieke (1995) obtained JK photometry of Palomar 6 using the 2.3m telescope equipped with a 256×256 HgCdTe NICMOS3 array at the Steward Observatory. Their image scale was same as ours (0.60 arcsec pixel^{-1}), but their observations covered wider area (6.6×2.5 arcmin). To calibrate their photometry, they observed the standard stars of Elias et al. (1982). Since standard stars of Elias et al. are too bright for their telescope plus camera configuration, they defocused the telescope to prevent the saturation of bright stars on the detector. They also observed the globular cluster M22 during the same night and they made comparisons with that of Frogel, Persson, & Cohen (1983);

$$\begin{aligned} \Delta K_{MOR-FPC} &= -0.15 \pm 0.11 \qquad (n = 3), \\ \Delta J_{MOR-FPC} &= 0.19 \pm 0.15 \qquad (n = 4), \end{aligned} \tag{4}$$

where $\Delta K_{MOR-FPC}$ and $\Delta J_{MOR-FPC}$ refer to Minniti et al. minus Frogel et al. (The error is 1 σ level.) They noted that the differences are large because their common stars are typically bright and close to the nonlinear regime of the detector array.

We compare our photometry with that of Minniti et al. in Figure 6. The differences are in the sense our photometry minus that of Minniti et al. We compared 134 common bright stars ($K \leq 12$ mag in our magnitude scale), and obtained unexpected results.

(i) On average, our K magnitudes are 1.384 $\pm$ 0.024 mag brighter than those of Minniti et al. (The error is that of the mean.) There exists a gradient in the difference with a slope of $\Delta K \propto 0.099 \times K$, in the sense that our K magnitudes are slightly brighter than the mean value for the bright stars.

(ii) On average, our J magnitudes are 0.705 $\pm$ 0.021 mag brighter than those of Minniti et al. There also exists a gradient in the difference with a slope of $\Delta J \propto 0.108 \times J$, in the sense that our J magnitudes for the bright stars are slightly brighter than the mean value.

(iii) Our $(J - K)$ colors are 0.679 $\pm$ 0.017 mag redder than those of Minniti et al.

The discrepancies between our work and Minniti et al. are too large to be fully explained by the differences between Minniti et al. and Frogel et al. in M22. We also show CMDs using common stars between our work and Minniti et al. in Figure 7. In the Figure, the left panel represents our photometry and right panel represents that of Minniti et al.[7]

[7]Dr. Minniti kindly provided his table for Palomar 6. A part of his table is shown below. His $(J - K)$ color values in the sixth column are 0.6 mag larger than those from the fifth column minus the fourth column. In Figure 7, we adopted the color from the fifth column minus the fourth column. Note that Minniti et al. (1995) used the color in the sixth column in their Figure 3.

X	Y	r	K	J	$(J-K)$	σK	σJ
190.8	321.0	1.30	10.65	11.47	1.42	0.01	0.01
194.2	323.6	5.60	12.54	13.62	1.68	0.04	0.04
182.5	315.5	8.70	13.92	14.94	1.62	0.11	0.13
189.0	310.9	9.20	10.05	11.04	1.59	0.01	0.01
....							

The off-cluster field star contamination is expected to be very high toward Palomar 6, as discussed in the previous section, and it is necessary to know membership RGB stars in our study. On 23 May 1998, we obtained high resolution ($\lambda/\Delta\lambda \geq$ 40,000) IR echelle spectra of 7 bright RGB stars in Palomar 6 and Arcturus for the ^{12}CO 2-0 bandhead centered at $\approx$ 22045 Å using the 3.5m NASA Infrared Telescope Facilities. In order to derive the heliocentric radial velocities, we cross-correlated our target spectra with that of Arcturus (v_r = -5.2 km sec^{-1}, Evans 1967). Table 3 shows our heliocentric radial velocity measurements for Palomar 6 RGB stars (see also Figure 3). The third column of the Table shows the membership of RGB stars based on their heliocentric radial velocities. (Hereafter, we refer stars A, C, D, and G as membership RGB stars.) It should be noted that the previous radial velocity of Palomar 6 is based on the low resolution spectroscopic study of Minniti (1995), where the internal measurement error is much larger than ours. We will discuss the spectroscopic study of Palomar 6 RGB stars in a forthcoming paper (Lee, Carney, & Balanchandran 2002, in preparation).

In Figure 8, we show $VJHK$ multi-color CMDs for Palomar 6, combining our JHK photometry and V photometry of Ortolani et al. (1995). Since we already knew the four cluster membership RGB stars (filled circles in the Figure), we drew RGB/RHB fiducial sequences with arbitrary widths in the ($V-K$, V) CMD by eye in the extension of the four membership RGB stars. We then removed outliers by cross-examining $H-K$ and $J-K$ colors. The remaining stars (likely the cluster membership stars) are plotted by crosses in the Figure. Our ($V-K$, K) and ($V-K$, V) CMDs may show that our JHK photometry shown in Figure 5 suffers a serious field star contamination, which is an expected result since Palomar 6 lies near the Galactic center. The RGB stars are clearly separated into at least 3 distinctive branches in ($V-K$, K) and ($V-K$, V) CMDs, in which the cluster's RGB stars are located to the blue indicating that Palomar 6 is more metal-poor or less heavily reddened than the surrounding fields.

In Figure 9, we show ($V-I$, V) CMDs for 47 Tuc (Kaluzny et al. 1998) and Palomar 6 (Ortolani et al. 1995). For the 47 Tuc CMD, we show a model isochrone for [Fe/H] = -0.83 and [α/Fe] = $+0.30$ (Bergbusch & VandenBerg 2001) and the location of RHB stars in 47 Tuc (see also Figure 34 of VandenBerg 2000). For the Palomar 6 CMD, filled circles are for Palomar 6 membership RGB stars, crosses for stars selected from multi-color CMDs (see Figure 8), and gray dots for stars within 1 arcmin from the cluster center. Since the model isochrone provides an excellent match with 47 Tuc, we adopt this model isochrone as a fiducial sequence for 47 Tuc. We then derived the relative distance modulus and interstellar reddening for Palomar 6 with respect to those for 47 Tuc by adjusting this model isochrone's magnitude to match with those of four Palomar 6 RGB stars (filled circles) and the model isochrone's color to match with the color that Ortolani et al. (1995) obtained at the intersection between the RHB and the RGB. The crossing point between the two dashed lines centered at V = 19.7 mag and $V - I$ = 2.7 mag indicates the RHB magnitude obtained by Ortolani et al. (1995). The color difference $\Delta(V - I)$ = 1.65 mag is corresponding to $\Delta E(B - V)$ = 1.27 mag, assuming $E(V - I) = 1.3E(B - V)$, and the magnitude difference ΔV = 5.1 mag corresponds to $\Delta(m - M)_0$ = 1.16 mag, in the sense of Palomar 6 minus 47 Tuc. It should be noted that the RHB magnitude reported by Ortolani et al. (1995) appears to be $\approx$ 0.4 - 0.5 mag fainter than that expected from 47 Tuc (the closed box at $V \approx 19.2$). Using these relative distance modulus and interstellar reddening values, we compare JK photometry for 47 Tuc and Palomar 6 in Figure 10. The filled circles are for the 47 Tuc RGB/RHB stars (Frogel et al. 1981) and dotted lines at $K \approx 6.5$ mag represent the RGB-tip K magnitude for 47 Tuc (Ferraro et al. 2000). The colors and the magnitudes of the current work (a) and those of Minniti et al. (b) are shifted by $\Delta(J - K) = -0.67$ mag and ΔK = 1.60 mag, assuming $\Delta E(B - V)$ = 1.27 and $\Delta(m - M)_0$ = 1.16 mag between Palomar 6 and 47 Tuc. In Figure 10-(a), we also show the mean magnitude and color of the Palomar 6 RHB stars (see below). Our RGB-tip K magnitude appears to be consistent with that of 47 Tuc, while that of Minniti et al. (1995) appears to be $\approx$ 1.5 mag fainter than 47 Tuc.

A comparison with 2 MICRON ALL-SKY SURVEY (2MASS, Curtri et al. 2000) may also provide an opportunity to assess our photometry, although 2MASS may have a potential problem in crowded fields due to a larger pixel scale (2 arcsec pixel^{-1}). Figure 11 shows a comparison of our photometry with that of 2MASS. Since 2MASS employed the K_S passband, we converted our magnitudes and colors into those of the 2MASS photometric system using the transformation relations given by Carpenter (2001). The results are

$$\begin{aligned} \Delta K_S &= -0.010 \pm 0.021, \\ \Delta(J - K_S) &= -0.152 \pm 0.018, \\ \Delta(H - K_S) &= -0.070 \pm 0.020, \end{aligned} \tag{5}$$

where the difference are in the sense our work minus 2MASS in the 2MASS photometric system. (The errors are those of the mean.) The difference in the $(J - K_S)$ color is rather large, in the sense that our photometry is $\approx$ 0.15 mag bluer than that of 2MASS, but the differences are much smaller than 1.4 mag in the K_S passband or 0.7 mag in the $(J - K_S)$ color.

Finally, we observed the four high proper motion stars (LHS 514, 2584, 2824, and 3094) during the same night. Table 4 shows a comparison of the unpublished results of Carney and our measurements. As can be seen in the Table, our measurements are in good agreement with that of Carney to within 0.1 mag. Therefore we conclude that the discrepancy between our work and that of Minniti et al. (1995) is most likely due to the inaccurate photometric measurement by Minniti et al. (1995).

3.3. Distance modulus and interstellar reddening

We derive the distance modulus and the interstellar reddening for Palomar 6 using the method described by Kuchinski et al. (1995), who recommended to use the magnitude and the color at the intersection between the RGB and the RHB in IR photometry. In Figure 12, we show the JK CMD for 47 Tuc of Frogel et al. (1981). We also show the slope of the RGB and the mean RHB magnitude and color. Kuchinski et al. (1995) obtained $(J-K)_{(RGB,RHB)}$ = 0.55 mag and $K_{(RGB,RHB)}$ = 12.02 mag at the intersection point between the RGB and RHB for 47 Tuc. Following the similar method, we derived these values for Palomar 6, using the possible membership stars obtained from Figure 8. First, we derive the slope of the Palomar 6 RGB stars

$$(J-K) = -0.0751\ (\pm 0.0040) \times K + 2.2030\ (\pm 0.0452). \tag{6}$$

We then define a rectangle whose sides are parallel to $J-K$ and K by eye and calculate the mean color and magnitude. We obtain $\langle J-K \rangle_{RHB} = 1.09 \pm 0.04$ mag and $\langle K \rangle_{RHB} = 13.53$ $\pm$ 0.15 mag for Palomar 6. (The error is 1 σ level.) In Figure 12, we show the slope of the RGB, the rectangle that we adopted and the mean RHB color and magnitude for Palomar 6. We obtain $(J-K)_{(RGB,RHB)} = 1.19$ mag for Palomar 6 using Equation 6.

By comparing the magnitudes $K_{(RGB,RHB)}$ and the colors $(J-K)_{(RGB,RHB)}$ at the RGB/RHB intersection points between 47 Tuc and Palomar 6, we obtained $\Delta E(B-V) =$ 1.21 mag and $\Delta(m-M)_0 = 1.09$ mag, assuming $E(J-K) = 0.53E(B-V)$ and $A_K =$ $0.35E(B-V)$ (Rieke & Lebofsky 1985). Using the distance modulus $(m-M)_0 = 13.25$ mag and the interstellar reddening $E(B-V) = 0.04$ mag for 47 Tuc (Harris 1996), we obtained the interstellar reddening $E(B-V) = 1.25$ mag and the distance modulus $(m-M)_0 = 14.34$ mag for Palomar 6. We also derive these values using the JH CMD. We obtained $(J-H)_{(RGB,RHB)}$ = 0.52 mag and $H_{(RGB,RHB)}$ = 12.10 mag for 47 Tuc, and $(J-H)_{(RGB,RHB)}$ = 0.95 mag and $H_{(RGB,RHB)}$ = 13.77 mag for Palomar 6. Assuming $E(J-H) = 0.33E(B-V)$ and $A_H = 0.54E(B-V)$ (Rieke & Lebofsky 1985), we obtained $E(B-V) = 1.34$ mag and $(m-M)_0 = 14.22$ mag for Palomar 6. For our study, we adopt the mean values, $E(B-V)$ = 1.30 mag and $(m-M)_0 = 14.28$ mag for Palomar 6. Our interstellar reddening estimate for Palomar 6 shows good agreement with previous values. However, our distance modulus estimate is $\approx$ 0.5 mag smaller than that of Ortolani et al. (1995) who obtained $(m-M)_0 =$ 14.76 using the HB magnitude shown in Figure 8. Using our distance modulus, the distance of Palomar 6 from the sun is $\approx$ 7.2 kpc. The Galactocentric distance R_{GC} becomes 0.9 kpc if $R_0 = 8.0$ kpc (Reid 1993). Palomar 6 is clearly located in the Galaxy's central regions.

Finally, a caution is advised for using RHB magnitudes to estimate the distance modulus of the metal-rich globular clusters. Sandage (1990) studied the vertical height of the horizontal branch of the globular clusters as a function of metallicity. His study suggested that the vertical height of the HB increases with metallicity. For example, the vertical height of the 47 Tuc RHB is ≈ 0.7 mag in the visual passband. Palomar 6 is expected to have the similar value of the RHB vertical height (see his Figure 16). In our CMDs, the Palomar 6 RHB vertical height is ≈ 0.5 - 0.6 mag in the K passband. It should also be noted that the K_0 magnitude of field red clump stars in the Galactic bulge is ≈ 13 mag (Alves 2000), having similar magnitude to Palomar 6 RHB stars depending on the interstellar reddening toward field red clump stars. Thus accidental inclusion of field red clump stars in our Palomar 6 CMD could be high and future photometric study of the off-cluster field would be desirable.

3.4. Metallicity

Kuchinski et al. (1995) studied the slope of the RGB in the $(J-K, K)$ CMD as a reddening- and distance-independent metallicity index for metal-rich globular cluster systems. They derived a linear relation between metallicity and the slope of the RGB

$$[\mathrm{Fe/H}] = -3.09(\pm 0.90) - 24.85(\pm 8.90) \times (\mathit{RGB\ slope}), \tag{7}$$

where the slope of the RGB is defined to be $(J-K) \propto K \times (\mathit{RGB\ slope})$. Kuchinski & Frogel (1995) recalculated this linear relation with the addition of two more clusters and they obtained,

$$[\mathrm{Fe/H}] = -2.98(\pm 0.70) - 23.84(\pm 6.83) \times (\mathit{RGB\ slope}). \tag{8}$$

We derived the slope of RGB of Palomar 6 and our result is shown in Figure 11 and Equation 6. As Kuchinski et al. (1995) and Kuchinski & Frogel (1995) noted, the slope of the RGB does not depend on the interstellar reddening and, therefore, conversion to dereddened colors and magnitudes is not necessary. With our slope for Palomar 6, we obtained [Fe/H] = -1.22 ± 0.18 using Equation 7 (Kuchinski et al. 1995) and -1.19 ± 0.18 using Equation 8 (Kuchinski & Frogel 1995). It should be noted that our results are from selected Palomar 6 RGB stars as discussed in the previous section. If we use all RGB stars, [Fe/H] = -1.05 ± 0.19 using Equation 7 and -1.03 ± 0.19 using Equation 8 and they are slightly lower than those from selected RGB stars.[8]

[8]Referee kindly pointed out that the IR HB morphology of Palomar 6 may indicate that its metallicity is between M69 ([Fe/H] = -0.6) and NGC 6553 ([Fe/H] = -0.3) from Figure 1 of Ferraro et al. (2000). It should be noted that, however, the HB morphology is vulnerable to other effects besides metallicity (see for example Lee, Demarque, & Zinn 1994).

Our metallicity estimate for Palomar 6 is consistent with that of Malkan (1981), but does not agree with those of Zinn (1985), Ortolani et al. (1995) and Minniti (1995). The metallicity of Palomar 6 will be discussed in the subsequent paper. We obtained [Fe/H] of the three RGB stars in Palomar 6 using high-resolution ($\lambda/\Delta\lambda \geq$ 40,000) IR echelle spectra. Our metallicity of Palomar 6 using IR spectra is [Fe/H] = -1.08 ± 0.06, consistent with those derived from the slope of the RGB.

4. Summary

We have presented the JHK photometry of Palomar 6. Our photometric measurements range from the RGB-tip to $\approx$ 2 mag below the RHB. Our photometry does not agree with that of Minniti et al. (1995) and an independent study using the southern telescope facilities would be very desirable in the future.

We have discussed the distance modulus and interstellar reddening of Palomar 6 by comparing the mean magnitude and color of the RHB stars with respect to those of 47 Tuc. Our interstellar reddening estimate is consistent with previous values by others, while our distance modulus is slightly smaller than that of Ortolani et al. (1995), who obtained the distance modulus of Palomar 6 by using the similar method in the visual passband. Nevertheless, our study has suggested that Palomar 6 is clearly located in the Galaxy's central regions.

We have also discussed the metallicity of Palomar 6 using the slope of the RGB. Our metallicity estimate is in good agreement with that of Malkan (1981), but does not agree with those of Zinn (1985), Ortolani et al. (1995) and Minniti et al. (1995).

This is part of Ph.D. thesis work of J. -W. Lee at the University of North Carolina at Chapel Hill. J. -W. Lee thanks Dr. Dante Minniti for providing his photometric table. We also thank an anonymous referee for useful comments and a careful review of the paper. This research was supported by the National Aeronautics and Space Administration (NASA) grant number GO-07318.04-96A from the Space Telescope Science Institute, which is operated by the Association of Universities for Research in Astronomy (AURA), Inc., under NASA contract NAS 5-26555 and the National Science Foundation grants AST96$-$19381 and AST99$-$88156. Support for this work was also provided in part by the Creative Research Initiative Program of Korean Ministry of Science and Technology.

REFERENCES

Alves, D. R. 2000, ApJ, 539, 732

Bergbusch, P. A., & VandenBerg, D. A. 2001, ApJ, 556, 322

Bica, E., Claria, J. J., Piatti, A. E., & Bonatto, C. 1998, A&AS, 131, 483

Carpenter, J. M. 2001, AJ, 121, 2851

Casali, M. M., & Hawarden, T. G. 1992, UKIRT newsletter, 4, 33

Cutri, R. M., et al. 2000, 2MASS Second Incremental Data Release (Pasadena: Caltech)

Elias, J. H., Frogel, J. A., Matthews, K., & Neugebauer, G. 1982, AJ, 87, 1029

Evans, D. S. 1967, in Determination of Radial Velocities and ther Applications, IAU Symp. No. 30, 57

Faber, S. M., Friel, E. D., Burstein, D., & Gaskell, C. M. 1985, ApJS, 57, 711

Ferraro, F. R., Montegriffo, P., Origlia, L., & Fusi Pecci, F. 2000, AJ, 119, 1282

Frogel, J. A., Persson, S. E., & Cohen, J. G. 1981, ApJ, 246, 842

Frogel, J. A., Persson, S. E., & Cohen, J. G. 1983, ApJS, 53, 713

Harris, W. E. 1996, AJ, 112, 1487

Kaluzny, J., Kubiak, M., Szymanski, M., Udalski, A., Krzeminski, W., Mateo, M., & Stanek, K. Z., 1998, A&AS, 128, 19

Kuchinski, L. E., & Frogel, J. A. 1995, AJ, 110, 2844

Kuchinski, L. E., Frogel, J. A., Terndrup, D. M., & Persson, S. E. 1995, AJ, 109, 1131

Lee, J. -W., & Carney, B. W. 1999, AJ, 117, 2868

Lee, Y. -W., Demarque, P., & Zinn, R. 1994, ApJ, 423, 248

Malkan, M. A. 1981, in Astrophysical Parameters for Globular Clusters, IAU Colloquim No. 68, 533

Minniti, D. 1995, A&A, 303, 468

Minniti, D., Olszewski, E. W., & Rieke, M. 1995, AJ, 110, 1686

Ortolani, S., Bica, E., & Barbuy, B. 1995, A&A, 296, 680

Reid, M. J. 1993, ARA&A, 31, 345

Rieke, G. H., & Lebofsky, M. J. 1985, ApJ, 288, 618

Sandage, A. 1990, ApJ, 350, 603

Stetson, P. B. 1987, PASP, 99, 191

Stetson, P. B. 1990, PASP, 102, 932

Stetson, P. B. 1994, PASP, 106, 250

Stetson, P. B., 1995, DAOPHOTII User's Manual (Victoria: Dominion Astrophys. Obs.)

Turner, A. M. 1995, Cooking with ALLFRAME (Victoria: Dominion Astrophys. Obs.)

VandenBerg, D. A. 2000, ApJS, 129, 315

Zinn, R. 1980, ApJS, 42, 19

Zinn, R. 1985, ApJ, 293, 424

This preprint was prepared with the AAS LaTeX macros v5.0.

Table 1. Journal of observations

Band	t_{exp}	FWHM (arcsec)	Dither (arcsec)
J	0.5 × 5 sec	1.0	6, 10
	5.0 × 5 sec	1.0	6, 10
H	0.5 × 5 sec	1.0	6, 10
	5.0 × 5 sec	1.0	6, 10
K	0.5 × 5 sec	1.0	6, 10
	5.0 × 5 sec	1.0	6, 10

Table 2. Color-magnitude diagram data

ID	X	Y	K	$J-K$	$H-K$
47	186.657	16.844	10.204	1.426	0.244
71	237.766	25.472	10.717	1.353	0.278
4	224.406	28.821	8.015	1.441	0.279
64	196.970	46.016	10.482	1.379	0.243
8	258.721	49.039	8.204	1.634	0.388
69	29.972	52.933	10.506	1.565	0.334
5	249.247	62.583	7.786	1.701	0.476
48	165.293	69.201	10.202	1.461	0.250
31	174.410	73.902	9.614	1.462	0.257
1	221.751	80.466	7.995	1.402	0.329

Table 3. Heliocentric radial velocities of Palomar 6 RGB stars.

ID[1]	v_r (km/s)	Membership
A	185.3	Yes
B	26.7	No
C	173.5	Yes
D	186.8	Yes
E	−13.5	No
F	134.5	No
G	176.7	Yes
Mean	180.6 ± 6.5	

[1]See also Figure 3.

Table 4. Comparisons of K magnitudes of high proper motion stars

ID	Carney	This Work
LHS 514	9.19	9.174 ± 0.011
LHS 2584	12.38	12.342 ± 0.012
LHS 2824	9.75	9.841 ± 0.011
LHS 3094	12.25	12.216 ± 0.017

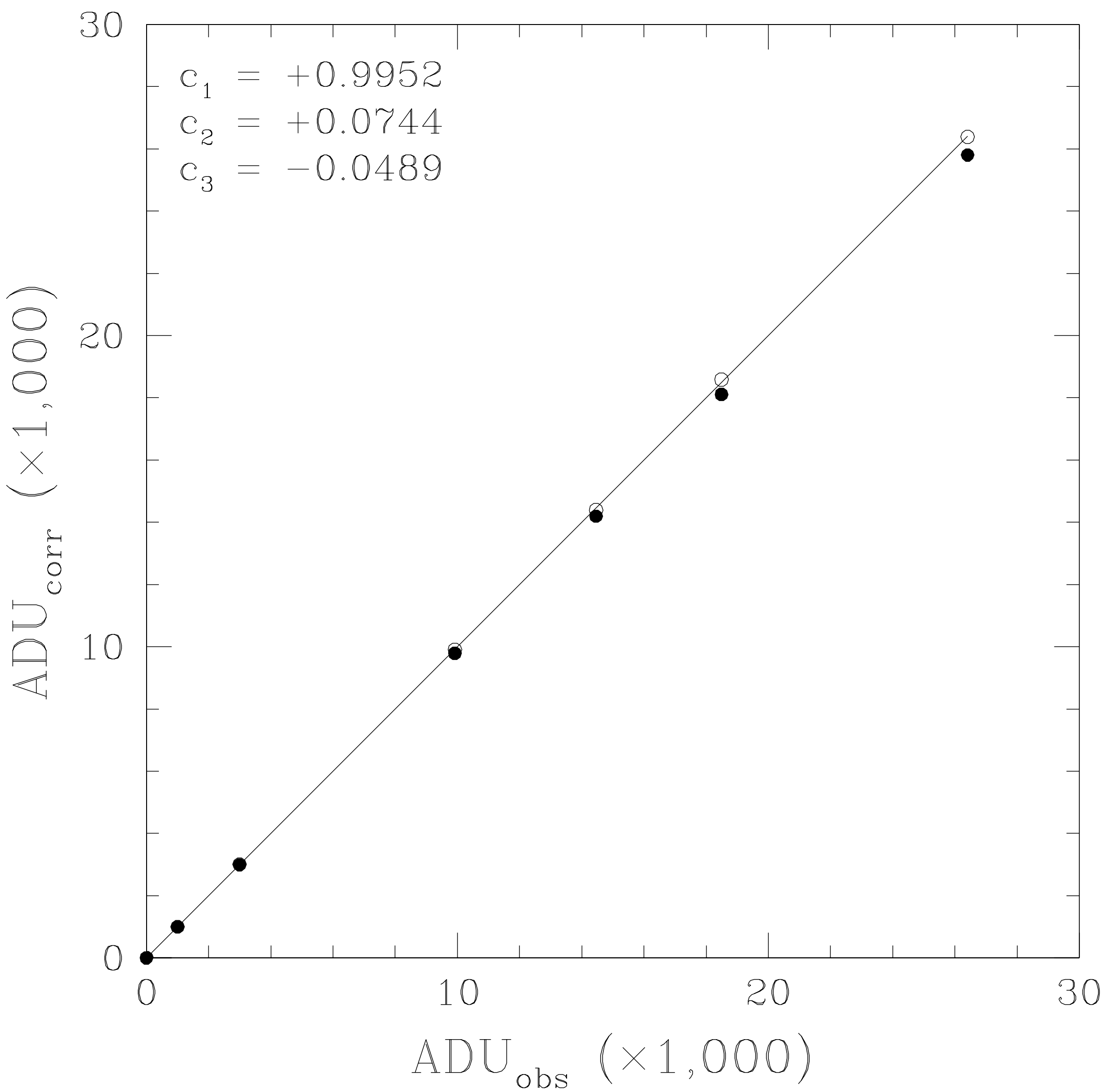

Fig. 1.— The non-linear response of NICMOS3 detector. The filled circles represent the observed fluxes and the open circles the corrected flux in ADU. The solid line represents the linear response function.

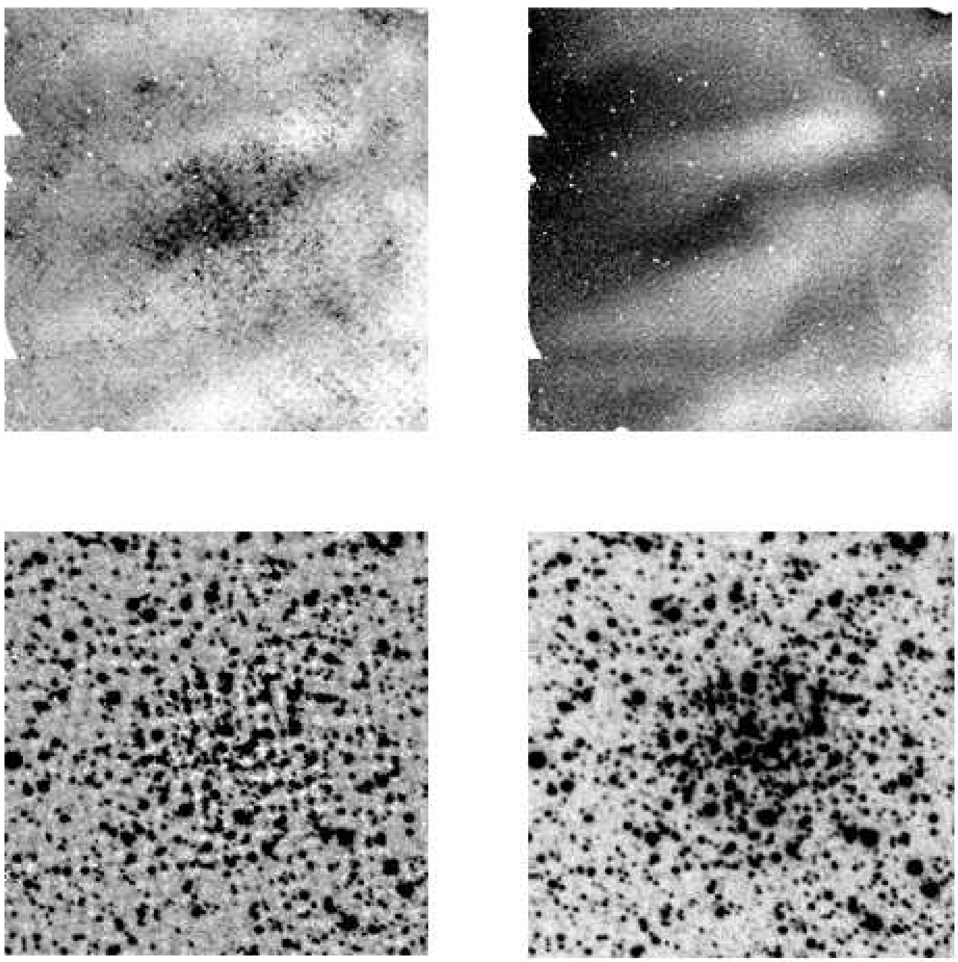

Fig. 2.— The upper left panel is the sky-flat generated from the Palomar 6 object frames and the upper right panel is the master sky-flat generated from the standard star frames. The upper left panel shows the residual light from stellar images especially in the central part of the frame. The lower panels represent the flat-field corrected images for each case.

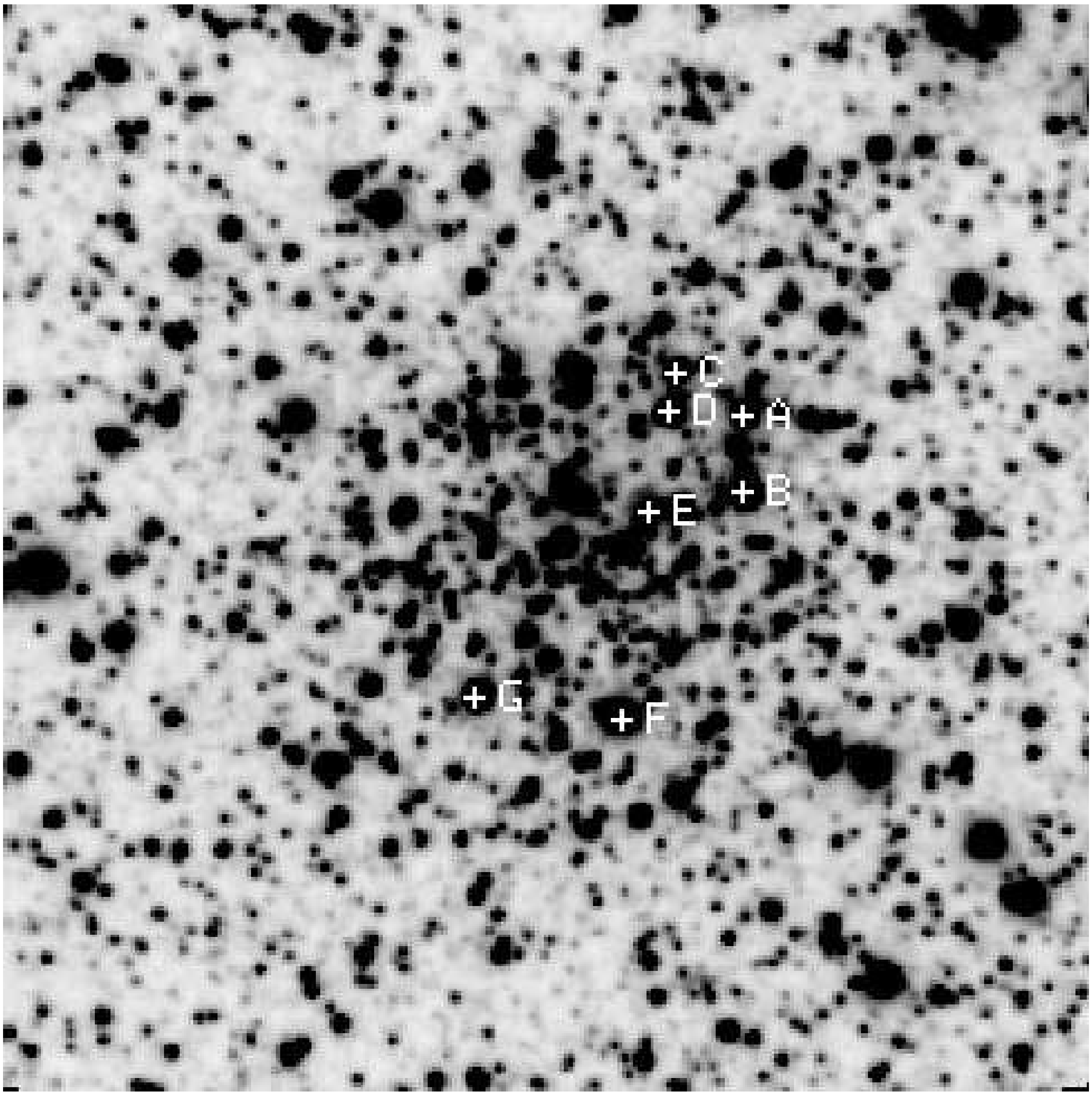

Fig. 3.— A composite image of Palomar 6 in K passband. North is at the top and east is to the left. The RGB stars with known heliocentric radial velocities in Table 2 are also marked.

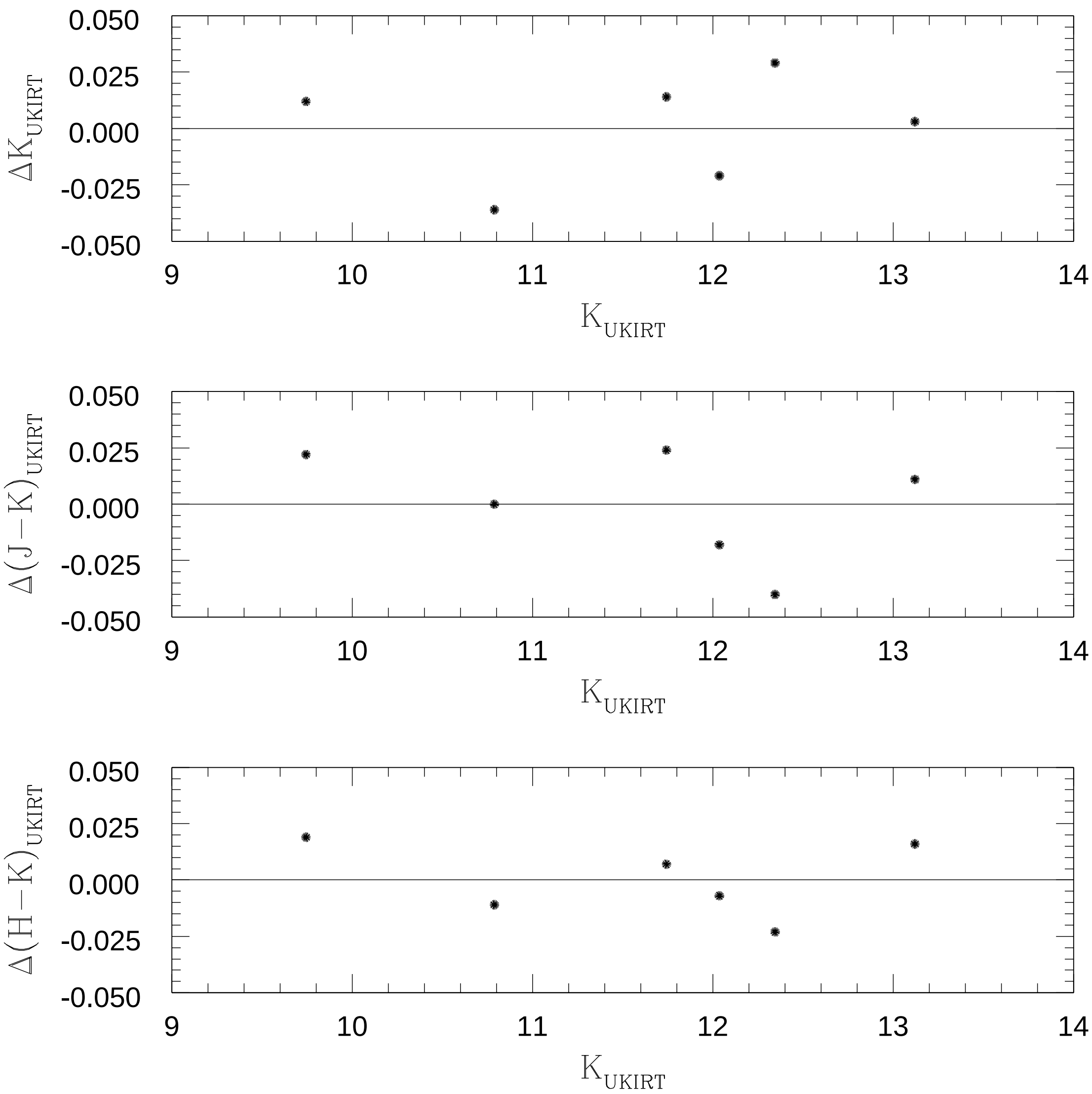

Fig. 4.— Transformation residuals of the UKIRT faint standard stars.

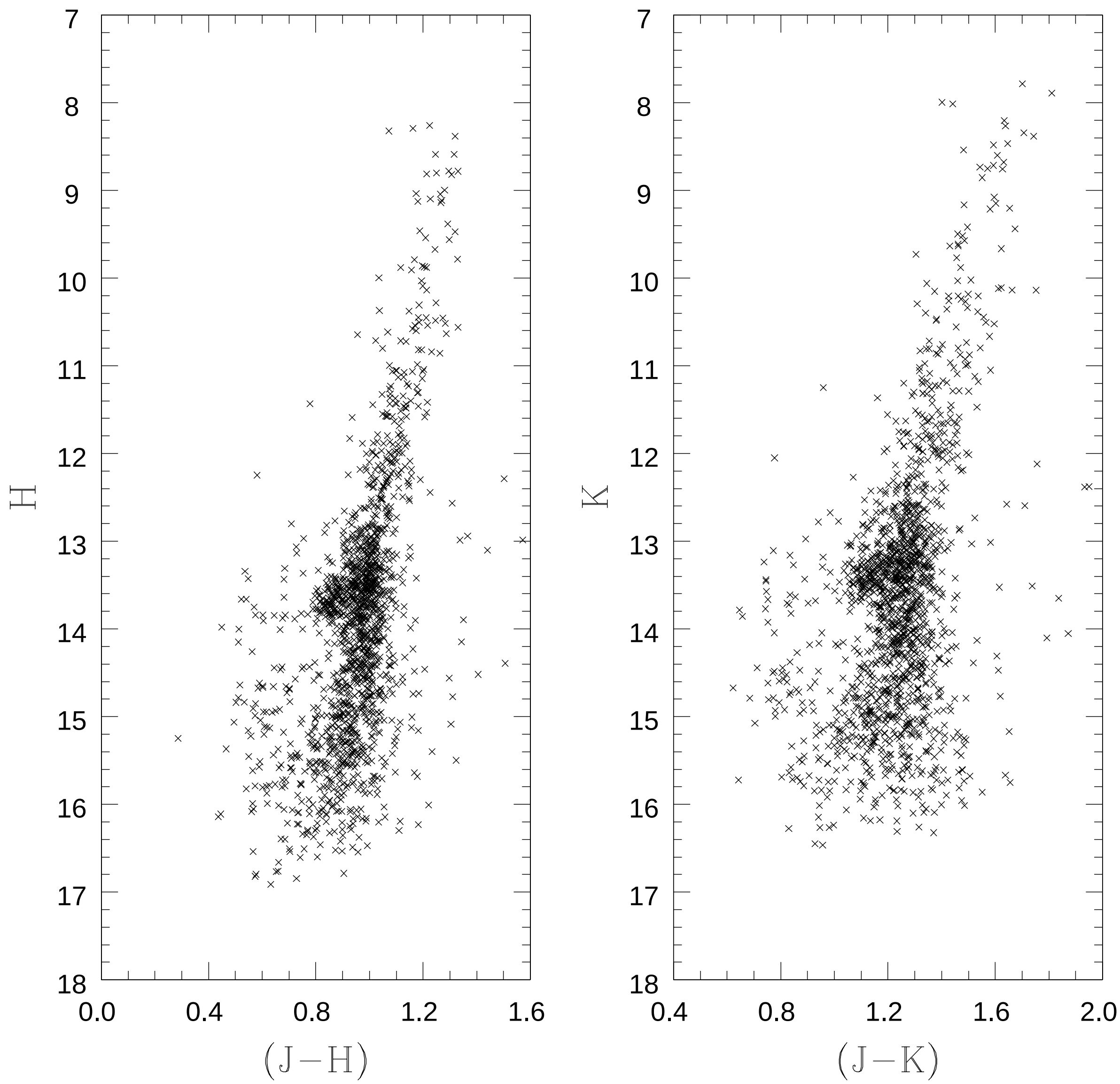

Fig. 5.— Composite IR CMDs of Palomar 6

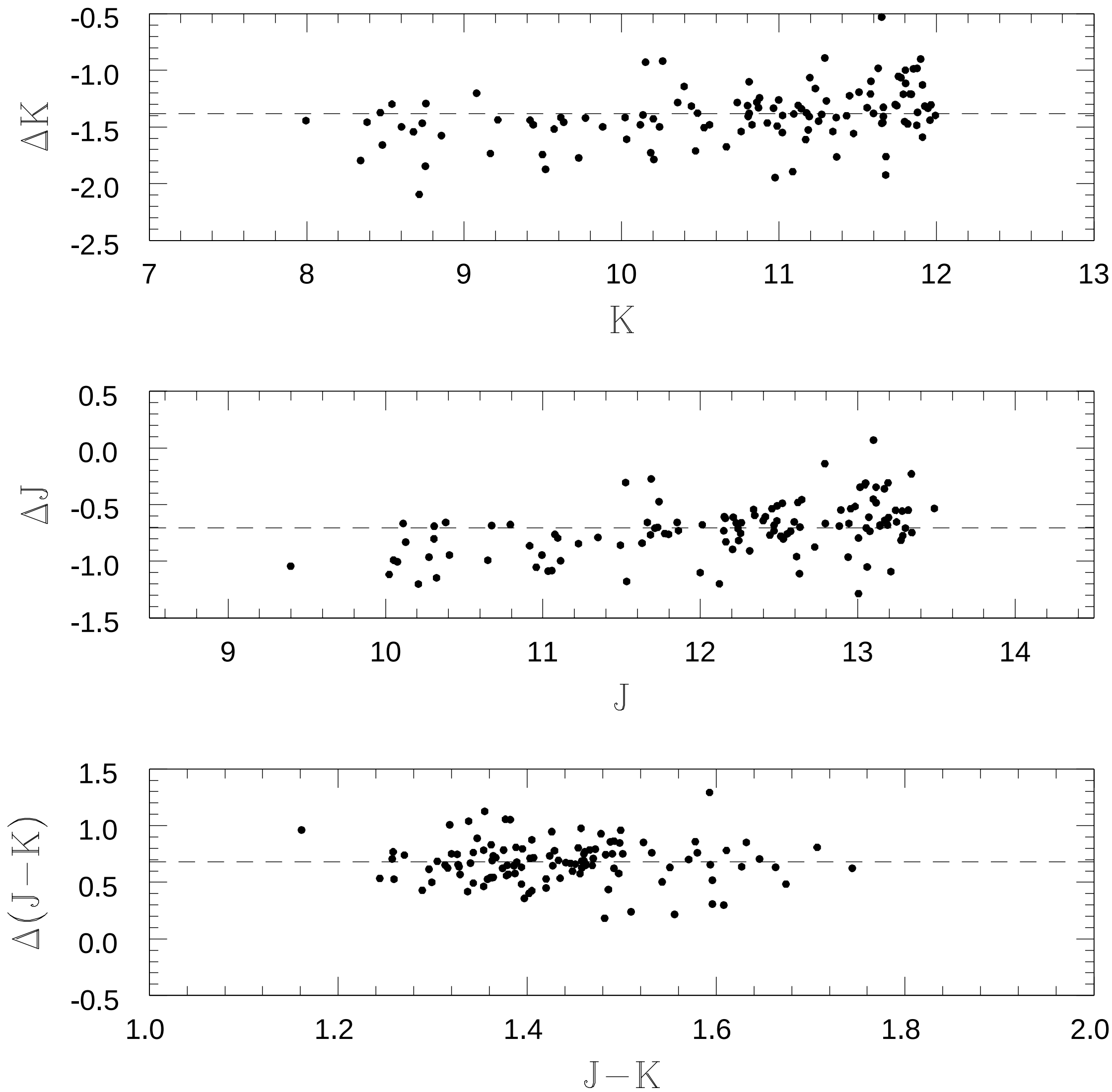

Fig. 6.— The residuals of the photometry between our work and Minniti et al. (1995). The differences are in the sense our photometry minus that of Minniti et al.

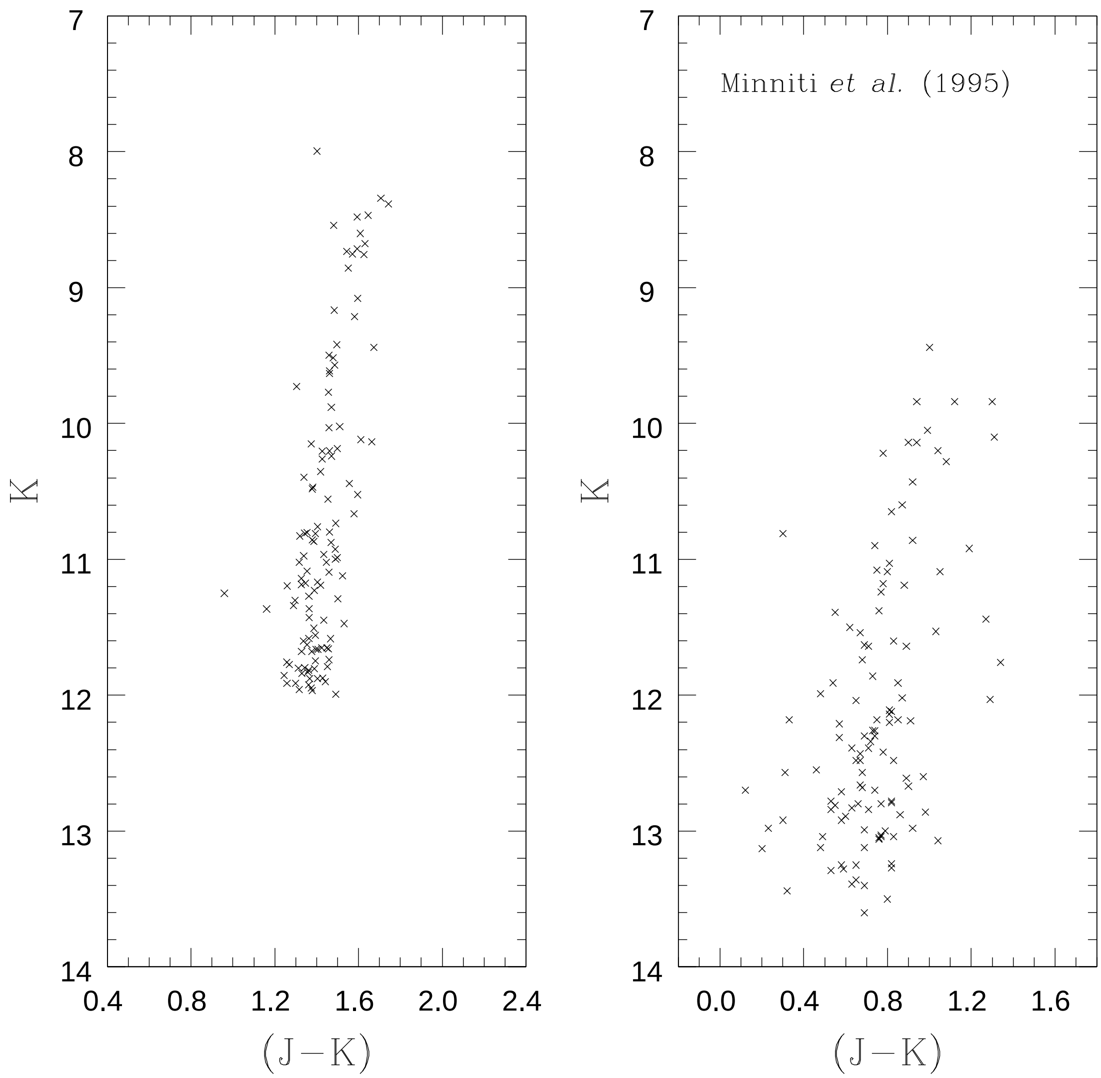

Fig. 7.— A comparison of CMDs using common stars between our work and Minniti et al.

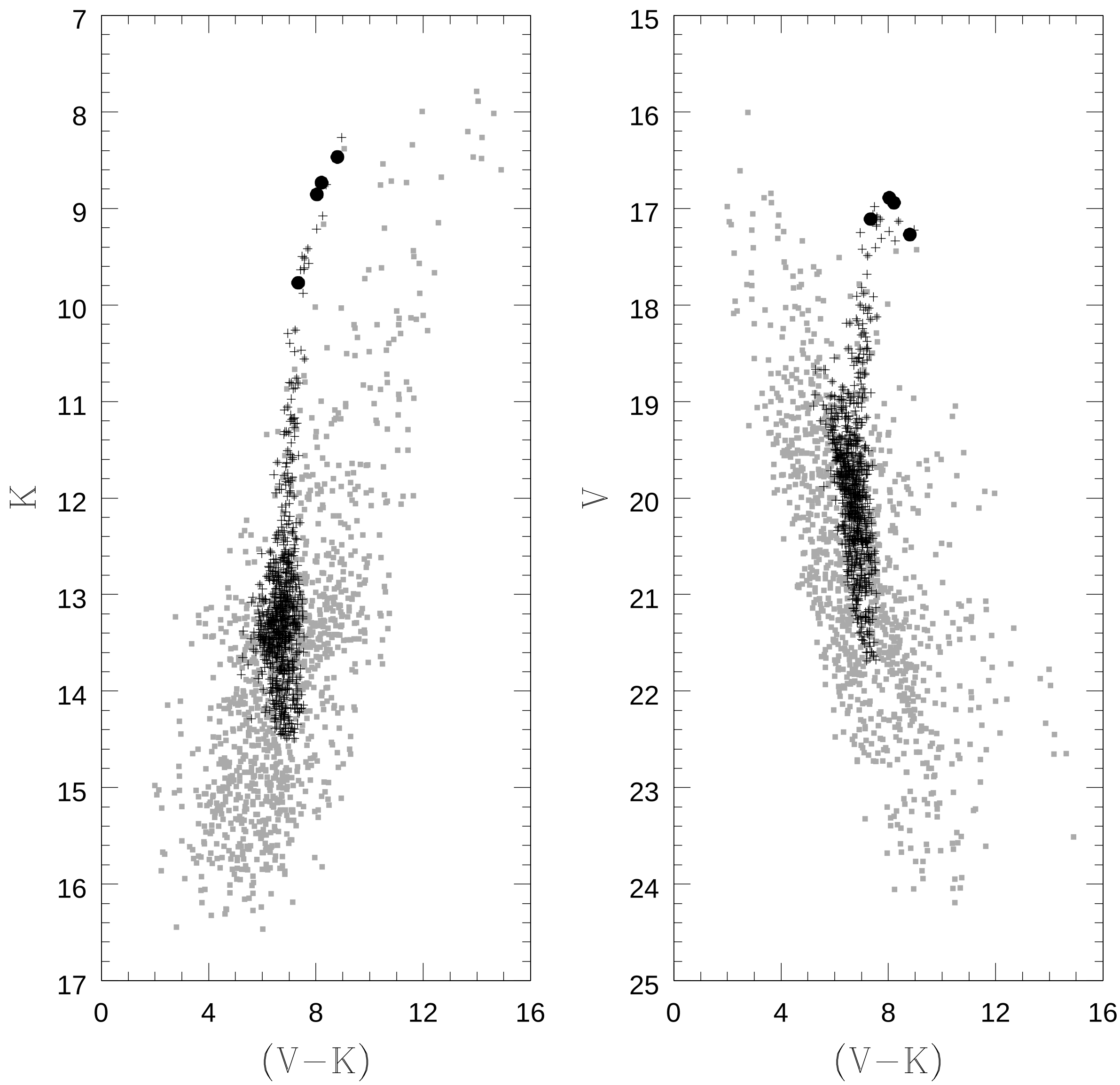

Fig. 8.— $VJHK$ multi-color CMDs of Palomar 6 and possible membership stars. Membership stars confirmed by radial velocity measurements are presented by filled circles and possible membership stars are presented by crosses.

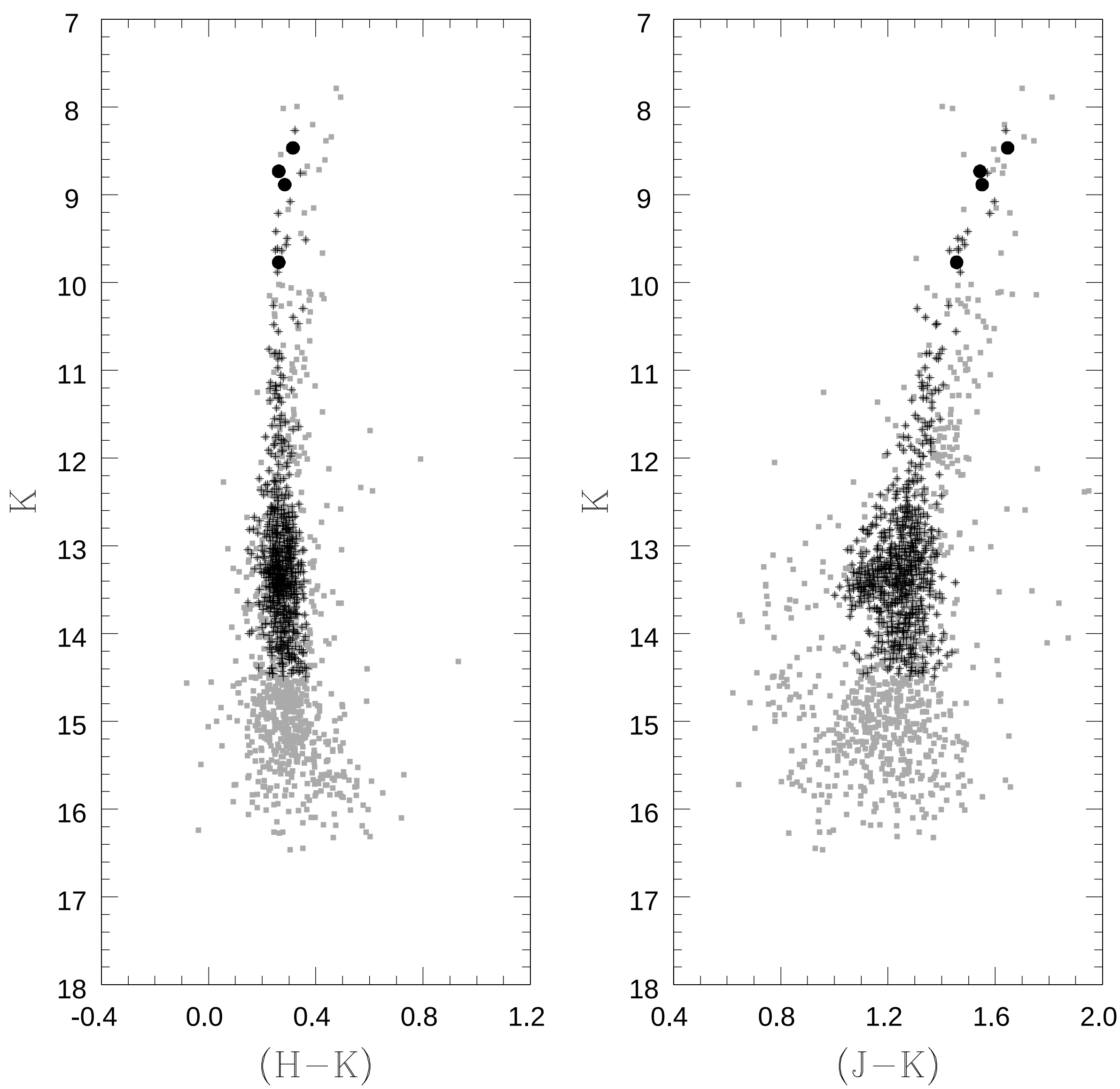

Fig. 8.— Continued.

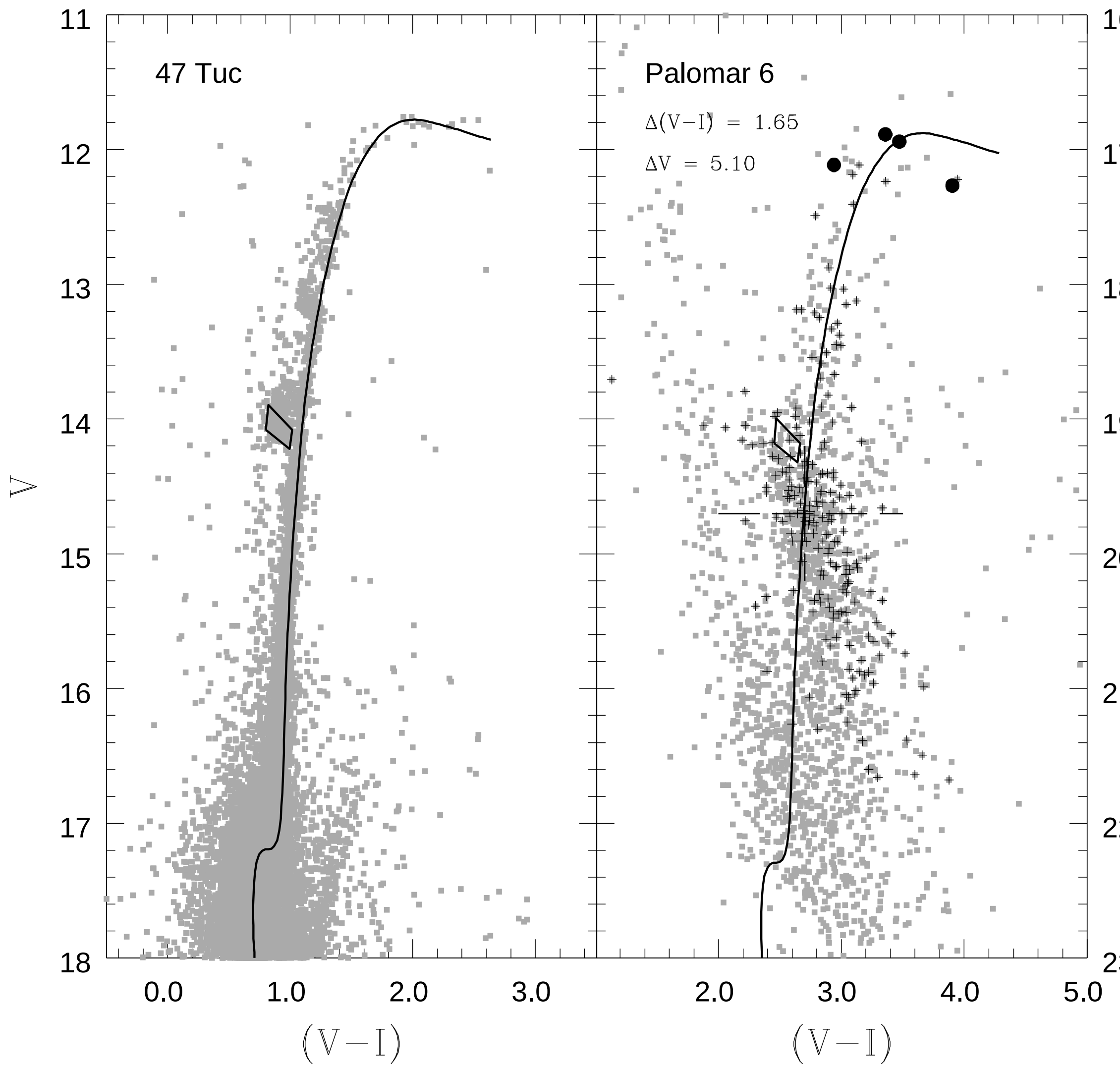

Fig. 9.— VI CMDs for 47 Tuc (Kaluzny et al. 1998) and Palomar 6 (Ortolani et al. 1995). We show a model isochrone for $[Fe/H] = -0.83$ and $[\alpha/Fe] = +0.30$ (Berbusch & VandenBerg 2001) and the location of RHB stars in 47 Tuc. Using this model isochrone, we derived the relative distance modulus and interstellar reddening for Palomar 6 with respect to those for 47 Tuc. In the right panel, filled circles are for Palomar 6 membership RGB stars, confirmed by radial velocity measurements, crosses for those selected using multi-color CMDs (see Figure 8), gray dots for stars within 1 arcmin from the cluster center, and the crossing point between the two dashed lines represnts the RHB magnitude by Ortolani et al. (1995). The color difference $\Delta(V - I) = 1.65$ is corresponding to $\Delta E(B - V) = 1.27$, assuming $E(V - I) = 1.3E(B - V)$, and the magnitude difference $\Delta V = 5.1$ mag is corresponding to $\Delta(m - M)_0 = 1.19$ mag, in the sense of Palomar 6 minus 47 Tuc.

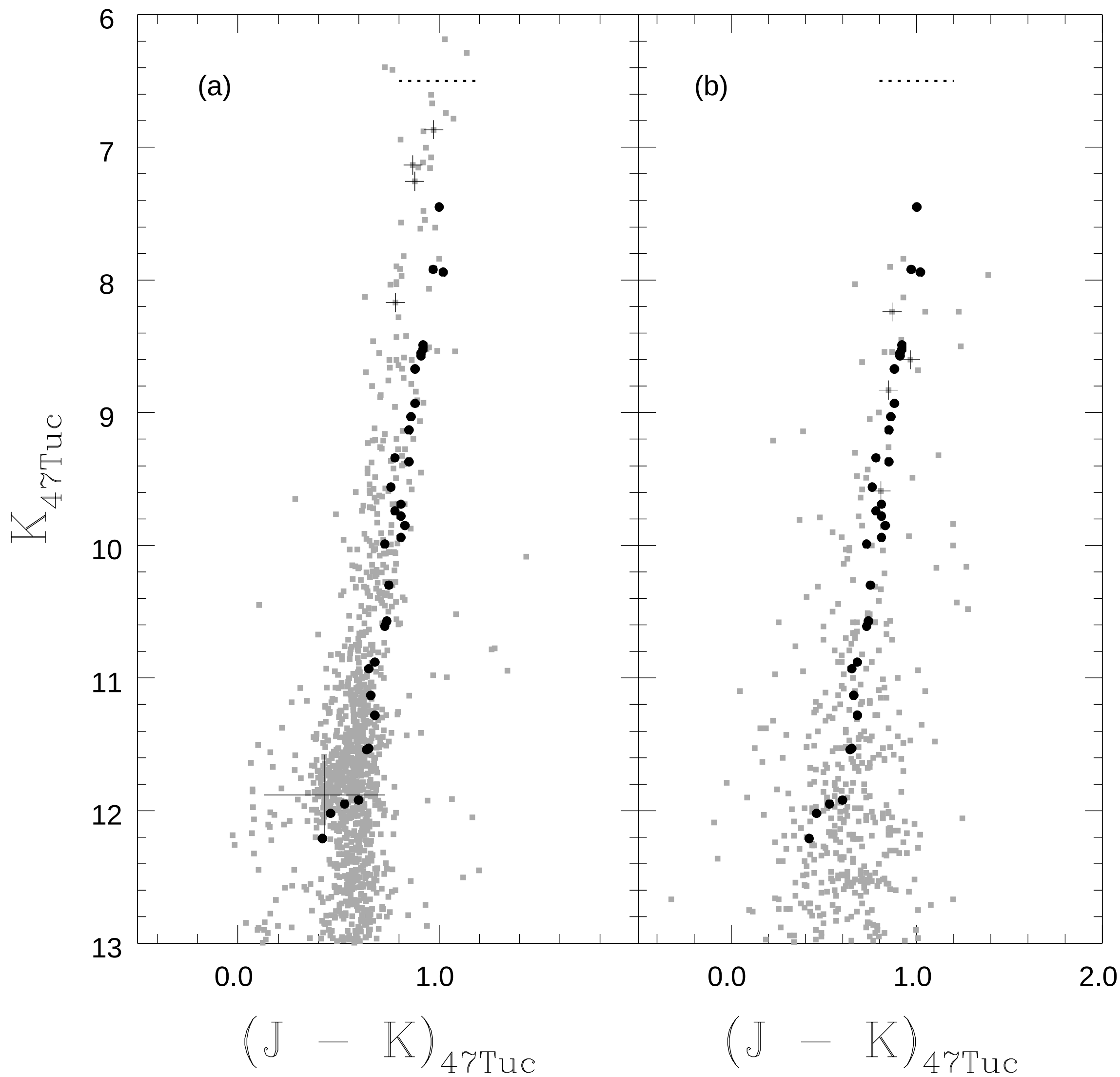

Fig. 10.— A comparison of JK photometry of Palomar 6 with respect to that of 47 Tuc. The filled circles are for the 47 Tuc RGB/RHB stars (Frogel et al. 1981) and dotted lines at $K \approx 6.5$ mag show the K magnitude of the brightest RGB stars in 47 Tuc (Ferraro et al. 2000). The colors and the magnitudes of the current work (a) and those of Minniti et al. (b) are shifted by $\Delta(J-K) = -0.67$ mag and $\Delta K = 1.60$ mag, assuming $\Delta E(B-V) = 1.27$ and $\Delta(m-M)_0 = 1.16$ mag between Palomar 6 and 47 Tuc. In Figure (a), we show the mean magnitude and color of the Palomar 6 RHB stars. The four membership RGB stars are represented by crosses in each panel. Our RGB-tip K magnitude is consistent with that of 47 Tuc, while that of Minniti et al. is ≈ 1.5 mag fainter than 47 Tuc.

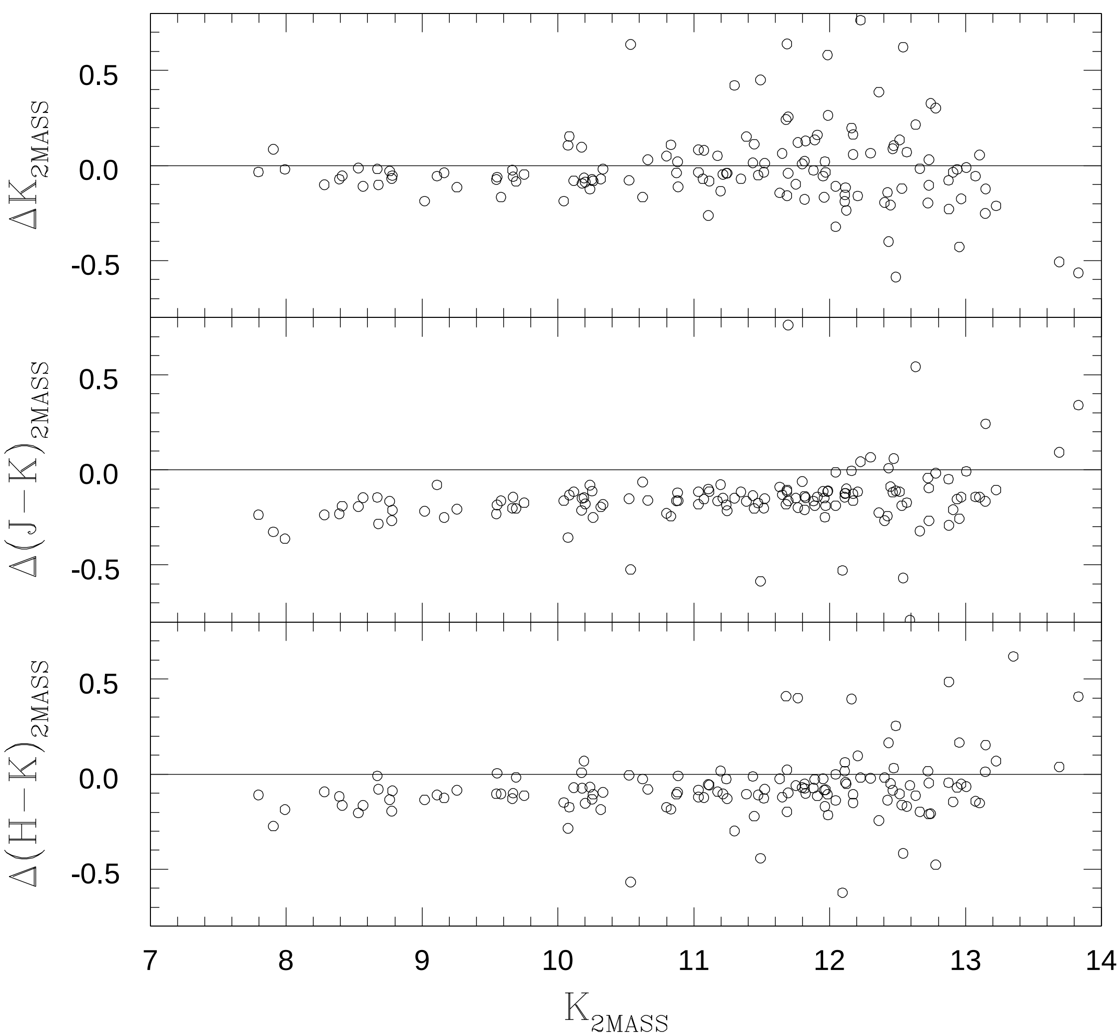

Fig. 11.— A comparison with 2MASS photometry. The differences are in the sense our photometry minus that of 2MASS.

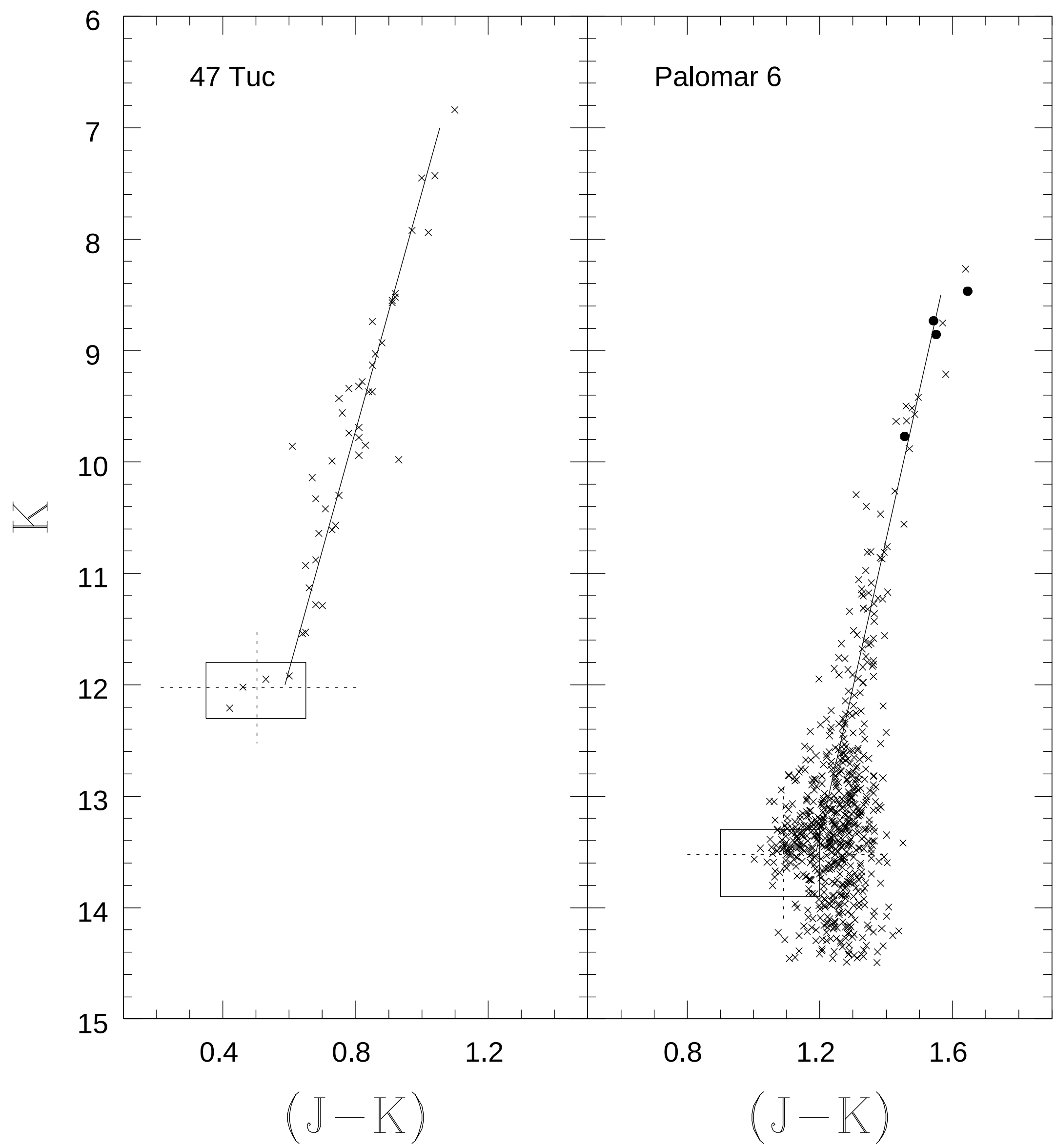

Fig. 12.— The mean RHB colors and magnitudes for Palomar 6 RHB and 47 Tuc. The center of the dotted lines represents the mean RHB color and magnitude, using stars inside the rectangle. The filled circles represent the Palomar 6 RGB membership stars.